Nuclear Engineering and Technology 51 (2019) 1479–1486

Contents lists available at ScienceDirect

Nuclear Engineering and Technology

journal homepage: www.elsevier.com/locate/net

Original Article

High accurate three-dimensional neutron noise simulator based on GFEM with unstructured hexahedral elements

Seyed Abolfazl Hosseini

Department of Energy Engineering, Sharif University of Technology, Tehran, 8639-11365, Iran

ARTICLE INFO

Article history:
Received 5 December 2018
Received in revised form
31 March 2019
Accepted 7 April 2019
Available online 9 April 2019

Keywords:
GFEM
Unstructured
Hexahedral
Tetrahedron
Noise source
Neutron noise distribution

ABSTRACT

The purpose of the present study is to develop the 3D static and noise simulator based on Galerkin Finite Element Method (GFEM) using the unstructured hexahedral elements. The 3D, 2G neutron diffusion and noise equations are discretized using the unstructured hexahedral by considering the linear approximation of the shape function in each element. The validation of the static calculation is performed via comparison between calculated results and reported data for the VVER-1000 benchmark problem. A sensitivity analysis of the calculation to the element type (unstructured hexahedral or tetrahedron elements) is done. Finally, the neutron noise calculation is performed for the neutron noise source of type of variable strength using the Green function technique.

It is shown that the error reduction in the static calculation is considerable when the unstructured tetrahedron elements are replaced with the hexahedral ones. Since the neutron flux distribution and neutron multiplication factor are appeared in the neutron noise equation, the more accurate calculation of these parameters leads to obtaining the neutron noise distribution with high accuracy. The investigation of the changes of the neutron noise distribution in axial direction of the reactor core shows that the 3D neutron noise analysis is required instead of 2D.

1. Introduction

Due to the importance of neutron noise analysis in the safety consideration of the reactor core and its application in calculating the kinetic parameters of the pressurized water reactor (PWR) or decay ratio in a Boiling Water Reactor (BWR) without causing perturbation in the reactor, the number of researches in this area has been increasing over the past years [1–4]. From the perspective of reactor safety analysis, timely identification of the accident symptoms as neutron noise source can prevent the occurrence of a severe accident. Properly un-located fuel assemblies in the reactor core, absorber of variable strength in the reactor core, very small changes in the absorption or scattering of the materials of the reactor core and vibration of control rods are examples of the neutron noise sources [4,5].

Earlier in the beginning of neutron noise analysis in 2004, 2D, 2G neutron noise equation was extracted by Demazière through the start of the time-dependent neutron diffusion equation, taking Fourier transform and some manipulation [6]. In the mentioned paper, the calculations were performed in the frequency domain via spatial discretization carried out by finite difference algorithm using rectangular meshes. Over time, many researchers developed different 2D neutron noise simulators using the various numerical discretization algorithms like Analytical Nodal Method (ANM), Galerkin Finite Element Method (GFEM) and Average Current Nodal Expansion Method (ACNEM) for rectangular and hexagonal geometries [7–12].

In the aforementioned published papers, the neutron noise sources were considered in the plate and 2D neutron noise distribution was calculated. Since the neutron noise can propagate to the plates other than the considered one, it seems reasonable to proceed with the study of noise in 3D. To this end, in the previous published study, 3D neutron noise computer code based on the GFEM with unstructured tetrahedron elements was developed [13]. The study showed that the neutron noise distribution in the axial direction changes both in the distribution and in the numerical value. Due to some advantages of the unstructured hexahedral elements and high accuracy of calculation using the hexahedral elements, the motivation of the present study is to develop the

E-mail addresses: sahosseini@sharif.edu, sahosseini@energy.sharif.edu.

https://doi.org/10.1016/j.net.2019.04.006

Abbreviations

3D	Three dimensional
2G	Two energy gropus
$\phi_g(r)$	Neutron flux in the energy group g
k_{eff}	Neutron multiplication factor
χ_g	Neutron spectrum in energy group g
D_g	Diffusion constant in the energy group g
$\Sigma_{r,g}$	Macroscopic removal cross section in the energy group g
$\Sigma_{f,g}$	Macroscopic fission cross section in the energy group g
$\Sigma_{s,g'\to g}$	Macroscopic scattering cross section from energy group g' to g
β_{eff}	Effective delayed neutron fraction
$C(r,t)$	Number of delayed neutron precursors
λ	Delayed neutron decay constant
ν	Fission neutron yield
∇	The nabla operator

neutron noise computer code based on GFEM using the unstructured hexahedral elements. Improvement of the results of static and noise calculation using the unstructured hexahedral elements in comparison to tetrahedral ones is the main purpose of the present study.

An outline of the remainder of this contribution is as follows: In Section 2, we briefly introduce the mathematical formulation used to develop the 3D neutron noise computer code by Galerkin finite element method with unstructured hexahedral elements. Section 3 presents the main specification of the VVER-1000 (3D) benchmark problems. Numerical results and discussion on results are presented in Section 4. Finally, Section 5 gives a summary and concludes the paper.

2. Mathematical formulation for the development of the neutron noise computer code

The time dependent neutron diffusion equation in two energy groups by considering the neutron energy spectrum as $\chi = \begin{bmatrix}1\\0\end{bmatrix}$ may be presented by Eq. (1) [14]:

$$\frac{1}{\nu_1}\frac{\partial}{\partial t}\varphi_1(r,t) = \nabla.D_1(r,t)\nabla\varphi_1(r,t) + \left[\left(1-\beta_{eff}\right)\nu\Sigma_{f,1}(r,t) - \Sigma_{a,1}(r,t) - \Sigma_{s,1\to2}(r,t)\right]\varphi_1(r,t) + \left(1-\beta_{eff}\right)\nu\Sigma_{f,2}(r,t)\,\varphi_2(r,t) + \lambda\,C(r,t) \quad (1)$$

$$\frac{1}{\nu_2}\frac{\partial}{\partial t}\varphi_2(r,t) = \nabla.D_2(r,t)\nabla\varphi_2(r,t) + \Sigma_{s,1\to2}(r,t)\,\varphi_1(r,t) - \Sigma_{a,2}(r,t)\,\varphi_2(r,t) \quad (2)$$

$$\frac{\partial}{\partial t}C(r,t) = \beta_{eff}\nu\Sigma_{f,1}(r,t)\,\varphi_1(r,t) + \beta_{eff}\nu\Sigma_{f,2}(r,t)\,\varphi_2(r,t) - \lambda\,C(r,t) \quad (3)$$

where, all the aforementioned parameters were defined in the abbreviation section. If the time dependent variables ($X(\vec{r},t)$)is separated to the average value (static state value) and perturbation ($\delta X(\vec{r},t)$) parts, it could be presented as Eq. (4):

$$X(\vec{r},t) = X(\vec{r}) + \delta X(\vec{r},t) \quad (4)$$

where, Xdenotes to the time dependent parameters like the neutron macroscopic cross sections and neutron flux. If the conditions given in Eq. (5) is valid, Eq. (6) that represents the first order neutron noise approximation will be achieved:

$$|\delta X(\vec{r},t)| << X(\vec{r}) \;and\; \langle\delta X(\vec{r},t)\rangle = 0 \quad (5)$$

$$\langle X(\vec{r},t)\rangle = X(\vec{r}) \quad (6)$$

To obtain the neutron noise equation based on the neutron diffusion equation, it is assumed that neutron macroscopic cross sections are perturbed due to agents like absorber of variable strength. Substituting Eq. (4) for all time dependent variables in Eqs. (1)–(3) gives the following equations:

$$\frac{1}{\nu_1}\frac{\partial}{\partial t}(\phi_1+\delta\phi_1) = \nabla.D_1\nabla(\phi_1+\delta\phi_1) + \left[\left(1-\beta_{eff}\right)\frac{\nu\Sigma_{f,1}+\delta\nu\Sigma_{f,1}}{k_{eff}} - \left(\Sigma_{R,1}+\delta\Sigma_{R,1}\right)\right](\phi_1+\delta\phi_1) + \left(1-\beta_{eff}\right)\frac{\nu\Sigma_{f,2}+\delta\nu\Sigma_{f,2}}{k_{eff}}(\phi_2+\delta\phi_2) + \lambda\,(C+\delta C) \quad (7)$$

$$\frac{1}{\nu_2}\frac{\partial}{\partial t}(\varphi_2+\delta\varphi_2) = \nabla.D_2\nabla(\varphi_2+\delta\varphi_2) + \left(\Sigma_{s,1\to2}+\delta\Sigma_{s,1\to2}\right)(\varphi_1+\delta\varphi_1) - \left(\Sigma_{a,2}+\delta\Sigma_{a,2}\right)(\varphi_2+\delta\varphi_2) \quad (8)$$

$$\frac{\partial}{\partial t}(C+\delta C) = \beta_{eff}\left[\frac{\nu\Sigma_{f,1}+\delta\nu\Sigma_{f,1}}{k_{eff}}(\varphi_1+\delta\varphi_1) + \frac{\nu\Sigma_{f,2}+\delta\nu\Sigma_{f,2}}{k_{eff}}(\varphi_2+\delta\varphi_2)\right] - \lambda\,(C+\delta C) \quad (9)$$

The static neutron diffusion equation is also given as Eqs. (10) and (11):

$$\nabla.D_1(r)\nabla\varphi_1(r) + \left[\frac{\nu\Sigma_{f,1}(r)}{k_{eff}} - \Sigma_{a,1}(r) - \Sigma_{s,1\to2}(r)\right]\varphi_1(r) + \frac{\nu\Sigma_{f,2}(r)}{k_{eff}}\varphi_2(r) = 0 \quad (10)$$

$$\nabla.D_2(r)\nabla\phi_2(r) + \Sigma_{s,1\to2}(r)\phi_1(r) - \Sigma_{a,2}(r)\,\phi_2(r) = 0 \quad (11)$$

Subtracting the static equations (Eq. (10) and (11)) from the time-dependent neutron diffusion equations (Eq. (7)–(9)), and eliminating the precursor density through a temporal Fourier transform, one obtains the first order approximation of the neutron noise equation as following [1,4,15–17]:

$$\nabla.D_1(r)\nabla\delta\phi_1(r,\omega)+\left(-\Sigma_{r,1}(r)-\frac{i\omega}{\nu_1}+\frac{\nu_1\Sigma_{f,1}(r)}{k_{eff}}\left(1-\frac{i\omega\beta_{eff}}{i\omega+\lambda}\right)\right)\delta\phi_1(r,\omega)+\frac{\nu_2\Sigma_{f,2}(r)}{k_{eff}}\left(1-\frac{i\omega\beta_{eff}}{i\omega+\lambda}\right)\delta\phi_2(r,\omega)=$$
$$\phi_1(r)\ \delta\Sigma_{s,1\to2}(r,\omega)+\phi_1(r)\delta\Sigma_{a,1}(r,\omega)-\phi_1(r)\left(1-\frac{i\omega\beta_{eff}}{i\omega+\lambda}\right)\delta\nu_1\Sigma_{f,1}(r,\omega)-\phi_2(r)\left(1-\frac{i\omega\beta_{eff}}{i\omega+\lambda}\right)\delta\nu_2\Sigma_{f,2}(r,\omega) \tag{12}$$

$$\nabla.D_2(r)\nabla\delta\phi_2(r,\omega)+\Sigma_{s,1\to2}(r)\delta\phi_1(r,\omega)+\left(-\Sigma_{a,2}(r)-\frac{i\omega}{\nu_2}\right)\delta\phi_2(r,\omega)$$
$$=-\phi_1(r)\ \delta\Sigma_{s,1\to2}(r,\omega)+\phi_2(r)\delta\Sigma_{a,2}(r,\omega) \tag{13}$$

where, $\delta\Sigma_{i,g}(r,\omega);\ i=a,f,s;\ g=1,2$denotes to the perturbation of absorption, fission and scattering cross sections in the fast and thermal energy groups, respectively. Also, $\nu_1$and ν_2, ω,β_{eff} and $\lambda$are the neutron velocity in the fast and thermal energy group, frequency of occurrence of the neutron noise source, effective delayed neutron fraction and decay constant, respectively.

As shown in Eqs. (12) and (13), the neutron flux distribution should be known to calculate the neutron noise source term. To this end, GFEM with unstructured hexahedral elements are used to calculate the neutron flux distribution into the reactor core. The same method is used to calculate neutron noise distribution via discretization of Eqs. (12) and (13). In order to avoid repeating the presentation of the discretization method for both of the static (solution of the neutron diffusion equation) and dynamical (solution of the neutron noise equation) calculations, only the discrete form of the neutron noise equation is presented. To solve the neutron noise equations (Eq. (12) and (13)), the Green's function technique is applied. In this study, it is assumed that the thermal macroscopic absorption cross section is perturbed. Therefore, the Green's function (neutron noise due to unit point neutron noise source) may be calculated by Eq. (14):

$$\left[\nabla.\overline{\overline{D}}(r)\nabla+\overline{\overline{\Sigma}}_{dyn}(r,\omega)\right]'\times\begin{bmatrix}G_{2\to1}\left(r,r',\omega\right)\\ G_{2\to2}r,r',\omega\end{bmatrix}=\begin{bmatrix}0\\ \delta\left(r-r'\right)\end{bmatrix} \tag{14}$$

where, $G_{2\to1}(r,r',\omega)$Gg→1r,r',ω and $G_{2\to2}(r,r',\omega)$Gg→2r,r',ω are the Green's function components in fast and thermal energy groups due to thermal neutron noise source, respectively. The $\overline{\overline{D}}(r)$and $\overline{\overline{\Sigma}}_{dyn}(r,\omega)$are defined as Eqs. (15) and (16):

$$\overline{\overline{D}}(r)=\begin{bmatrix}D_1(r) & 0\\ 0 & D_2(r)\end{bmatrix} \tag{15}$$

$$\overline{\overline{\Sigma}}_{dyn}=\begin{bmatrix}-\Sigma_1(r,\omega) & \frac{\nu_2\Sigma_{f,2}(r)}{k_{eff}}\left(1-\frac{i\omega\beta_{eff}}{i\omega+\lambda}\right)\\ \Sigma_{s,1\to2}(r) & -\left(\Sigma_{a,2}(r)+\frac{i\omega}{\nu_2}\right)\end{bmatrix} \tag{16}$$

where, we have:

$$\Sigma_1(r,\omega)=\Sigma_{a,1}(r)+\Sigma_{s,1\to2}(r)+\frac{i\omega}{\nu_1}-\frac{\nu_1\Sigma_{f,1}(r)}{k_{eff}}\left(1-\frac{i\omega\beta_{eff}}{i\omega+\lambda}\right) \tag{17}$$

The discrete form of Eq. (14) is presented as Eqs. (18) and (19) using GFEM:

$$\sum_{e=1}^{E}\left[\iiint_{V^{(e)}}dx\,dy\,dzD_1\ \nabla\overline{N}^{(e)}(x,y,z)\ \nabla\overline{N}^{(e)T}(x,y,z)G_{2\to1}^{(e)}-\Sigma_1^{(e)}\iiint_{V^{(e)}}dx\,dy\,dz\overline{N}^{(e)}(x,y,z)\overline{N}^{(e)T}(x,y,z)G_{2\to1}^{(e)}+\right.$$
$$\left.\frac{\nu_2\Sigma_{f,2}^{(e)}}{k_{eff}}\left(1-\frac{i\omega\beta_{eff}}{i\omega+\lambda}\right)\iiint_{V(e)}dx\,dy\,dz\,\overline{N}^{(e)}(x,y,z)\overline{N}^{(e)T}(x,y,z)G_{2\to2}^{(e)}+\iint_{S^{(e)}}ds\overline{N}^{(e)}(x,y,z)\overline{N}^{(e)T}(x,y,z)\frac{G_{2\to1}^{(e)}}{2}\right]=0, \tag{18}$$

$$\sum_{e=1}^{E}\left[\iiint_{V^{(e)}}dx\,dy\,dz\,D_2\ \nabla\overline{N}^{(e)}(x,y,z)\nabla\overline{N}^{(e)T}(x,y,z)G_{2\to2}^{(e)}+\Sigma_{s,1\to2}^{(e)}\iiint_{V^{(e)}}dx\,dy\,dz\,\overline{N}^{(e)}(x,y,z)\overline{N}^{(e)T}(x,y,z)G_{2\to1}^{(e)}-\right.$$
$$\left.\left(\Sigma_{a,2}^{(e)}+\frac{i\omega}{\nu_2}\right)\iiint_{V^{(e)}}dx\,dy\,dz\overline{N}^{(e)}(x,y,z)\overline{N}^{(e)T}(x,y,z)G_{2\to1}^{(e)}+\iint_{S^{(e)}}ds\overline{N}^{(e)}(x,y,z)\overline{N}^{(e)T}(x,y,z)\frac{G_{2\to2}^{(e)}}{2}\right]=\begin{bmatrix}N_1^{(e)}\left(x',y',z'\right)\\ .\\ .\\ .\\ N_8^{(e)}\left(x',y',z'\right)\end{bmatrix} \tag{19}$$

where, $N_i^{(e)}(x,y,z);\ i = 1,2,\ldots,8$are the shape function components in the hexahedral elements. The solution of the system of equations (18) and (19) leads to obtaining the Green function components. In the linear approximation of shape function in each element, the Green function components in the any point inside the hexahedral element are written as Eq. (20):

$$\phi^{(e)}(x,y,z) = N_1^{(e)}(x,y,z)\phi_1 + N_2^{(e)}(x,y,z)\phi_2 + \ldots + N_8^{(e)}(x,y,z)\phi_8 \tag{20}$$

After the calculation of Green function components, the fast and thermal neutron noise distribution due to thermal neutron noise source are calculated using the Eq. (21):

$$\begin{bmatrix} \delta\phi_1(r,\omega) \\ \delta\phi_2(r,\omega) \end{bmatrix} = \begin{bmatrix} \iiint_{V^{(e)}} G_{2\to1}\left(r,r',\omega\right) S_2\left(r,r',\omega\right) dV' \\ \iiint_{V^{(e)}} G_{2\to2}\left(r,r',\omega\right) S_2\left(r,r',\omega\right) dV' \end{bmatrix} \tag{21}$$

The complete solution of the neutron noise equation (based on GFEM with arbitrary unstructured hexahedral elements is so complicated. As shown in Fig. 1, to reduce the complexity of the solution, a mapping of the unstructured hexahedral elements from (x, y, z)coordinate to regular cube in (ξ, η, ζ)coordinate has been performed. The coordinates of the nodes in the coordinate system are given in Table 1.

Considering the properties of the shape function in each unstructured hexahedral element, the components of shape function in the new coordinate system may be written as Eq. (22):

$$\begin{aligned} N_1^e(\xi,\eta,\zeta) &= \frac{1}{8}(1\pm\xi)(1+\eta)(1-\zeta) \\ N_3^e(\xi,\eta,\zeta) &= \frac{1}{8}(1\pm\xi)(1+\eta)(1+\zeta) \\ N_5^e(\xi,\eta,\zeta) &= \frac{1}{8}(1\pm\xi)(1-\eta)(1-\zeta) \\ N_7^e(\xi,\eta,\zeta) &= \frac{1}{8}(1\pm\xi)(1-\eta)(1+\zeta) \end{aligned} \tag{22}$$

The coordinates of (x, y, z)inside the unstructured hexahedral elements is presented as Eq. (23):

$$n^{(e)} = \sum_{i=1}^{8} n_i L_i^{(e)}(\xi,\eta,\zeta) \tag{23}$$

where, n denotes to x, y or z and$(x_i,y_i,z_i)$are the coordinates of the vertices of the unstructured hexahedral elements. After calculation of the Jacobi for each element, the determinant of the Jacobi matrix of the hexahedral elements is finally calculated as Eq. (24):

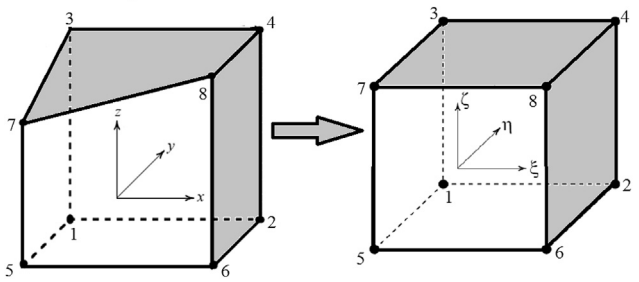

Fig. 1. Coordinate transformation from (x,y,z)coordinate to (ξ,η,ζ)

Table 1
The coordinates of the nodes in the new coordinate system.

node	1	2	3	4	5	6	7	8
ξ	−1	+1	−1	+1	−1	+1	−1	+1
η	+1	+1	+1	+1	−1	−1	−1	−1
ζ	−1	−1	+1	+1	−1	−1	+1	+1

$$\begin{aligned} |J| = {} & A + B\xi + C\eta + D\zeta + E\xi^2 + F\eta^2 + G\zeta^2 + H\xi\eta + I\eta\zeta + J\xi\zeta \\ & + K\eta\xi^2 + M\eta^2\zeta + N\eta\zeta^2 + O\xi^2\zeta + P\xi\zeta^2 + Q\eta^2\xi + R\eta\xi^2\zeta \\ & + S\eta^2\xi\zeta + T\eta\xi\zeta^2 + U\eta\xi\zeta \end{aligned} \tag{24}$$

where, the coefficients of Eq. (24) (A, B, …, U) have been defined vs. the coordinates of the hexahedral vertices.

To obtain the final form of the system of equations, the appeared integrals in Eqs. (18) and (19) should be solved. The first type of the appeared integrals in Eqs. (18) and (19) is as Eq. (25):

$$\begin{aligned} \bar{\bar{I}}_1^{(e)} &= \iiint_{V^{(e)}} dxdydz\overline{N}^{(e)}(x,y,z)\overline{N}^{(e)T}(x,y,z) \\ &= \int_{-1}^{1}\int_{-1}^{1}\int_{-1}^{1} \overline{N}^{(e)}(\xi,\eta,\zeta)\overline{N}^{(e)^T}(\xi,\eta,\zeta)|J|d\xi d\eta d\zeta \end{aligned} \tag{25}$$

where, the elements of $\bar{\bar{I}}_1^{(e)}$ matrix are calculated by considering Eqs. (22) and (24).

To solve the integral $\bar{\bar{I}}_2^{(e)} = \iiint_{V^{(e)}} dxdydz\nabla\overline{N}^{(e)}(x,y,z)\nabla\overline{N}^{(e)T}(x,y,z)$, it should be noted that $\begin{Bmatrix} \frac{\partial N_i}{\partial x} \\ \frac{\partial N_i}{\partial y} \\ \frac{\partial N_i}{\partial z} \end{Bmatrix} = J^{-1}\begin{Bmatrix} \frac{\partial N_i}{\partial \xi} \\ \frac{\partial N_i}{\partial \eta} \\ \frac{\partial N_i}{\partial \zeta} \end{Bmatrix}$. Therefore, we have Eq. (26):

$$\bar{\bar{I}}_2^{(e)} = \int_{-1}^{1}\int_{-1}^{1}\int_{-1}^{1} \left[J^{-1}.\nabla\overline{N}^{(e)}(\xi,\eta,\zeta)\right]\left[J^{-1}.\nabla\overline{N}^{(e)T}(\xi,\eta,\zeta)\right]|J|d\xi d\eta d\zeta \tag{26}$$

The Gauss-Legendre method [18] as Eq. (27) is used to solve the integral of Eq. (26):

$$\int_{-1}^{1}\int_{-1}^{1}\int_{-1}^{1} f(\xi,\eta,\zeta)d\xi d\eta d\zeta = \sum_{k=1}^{N}\sum_{j=1}^{N}\sum_{i=1}^{N} f\left(\xi_i,\eta_j,\zeta_k\right)w_i w_j w_k \tag{27}$$

where, $N = 2$, and w_i, $w_j$and $w_k$are obtained from the Gauss-Legendre weights.

The last integral is related to the boundary condition that is presented by $\bar{\bar{I}}_3^{(e)}$. For the no incoming current boundary condition, the local boundary condition matrix for each element is calculated as Eq. (28).

$$\bar{\bar{I}}_3^{(e)}(1,1)=\frac{1}{9}(\delta_2-\delta_1+2\delta_0);\bar{\bar{I}}_3^{(e)}(1,2)=\frac{1}{18}(\delta_2+2\delta_0)$$

$$\bar{\bar{I}}_3^{(e)}(1,2)=-\frac{1}{18}(\delta_1-2\delta_0);\bar{\bar{I}}_3^{(e)}(1,6)=\bar{\bar{I}}_3^{(e)}(2,5)=\frac{\delta_0}{18}$$

$$\bar{\bar{I}}_3^{(e)}(2,2)=\frac{1}{9}(\delta_2+\delta_1+2\delta_0);\bar{\bar{I}}_3^{(e)}(2,6)=\frac{1}{18}(\delta_1+2\delta_0)$$

$$\bar{\bar{I}}_3^{(e)}(5,5)=\frac{1}{9}(\delta_1+\delta_2-2\delta_0);\bar{\bar{I}}_3^{(e)}(5,6)=\frac{1}{18}(\delta_2-2\delta_0)$$

$$\bar{\bar{I}}_3^{(e)}(6,6)=\frac{1}{9}(\delta_1-\delta_2+2\delta_0) \quad (28)$$

where, the matrix is symmetric and the rest of its element are zero. The determinant of Jacobi of the unstructured quadrilateral surface elements is defined as Eq. (29):

$$|J'|=\delta_0+\delta_1\xi+\delta_2\eta \quad (29)$$

Substitution of the aforementioned matrices in Eqs. (18) and (19) and solution of the system of equations leads to calculate the Green function components. After the calculation of Green function components, the fast and thermal neutron noise distributions are calculated by an integral over the source and the Green's function as Eq. (21).

3. Main specification of the benchmark problems

To validate the calculations, the VVER-1000 reactor core [19] was considered. To solve the three-dimensional neutron diffusion equation, the neutron diffusion coefficients and neutron macroscopic cross sections given in Table 2 for VVER-1000 reactor core were used. The considered geometry of VVER-1000 reactor core in the simulation was displayed in Fig. 2. As shown, the boundary conditions of the reactor core in the simulation is vacuum.

Table 2
The material cross section of each assembly for VVER-1000 reactor core.

Fuel assembly No.	(1)	(2)	(3)	(4)	(5)	(6)	(7)
$\nu\Sigma_{f,1}(cm^{-1})$	0.005	0.005	0.006	0.006	0.006	0.000	0.006
$\nu\Sigma_{f,2}(cm^{-1})$	0.084	0.084	0.115	0.126	0.130	0.000	0.126
$\Sigma_{a,1}(cm^{-1})$	0.008	0.010	0.009	0.010	0.009	0.016	0.009
$\Sigma_{a,2}(cm^{-1})$	0.066	0.075	0.080	0.095	0.088	0.053	0.086
$\Sigma_{s,1\to2}$	0.016	0.014	0.015	0.014	0.015	0.025	0.015
$D_1(cm)$	1.375	1.409	1.371	1.394	1.369	1.000	1.369
$D_2(cm)$	0.383	0.388	0.380	0.385	0.379	0.333	0.379

4. Results

In the present paper, to avoid repeating the description of how to calculate neutron flux distribution, only the solution of the neutron noise equation using GFEM with unstructured hexahedral elements was explained. The neutron diffusion equation may be solved by the same algorithm (GFEM). Similar to the neutron noise equation, three types of integrals were appeared in discrete form of the neutron diffusion equation. The static calculation were repeated for the five different number of the unstructured hexahedral elements in the reactor core. Table 3 compares the calculated neutron multiplication factors with their Relative Percent Error (RPE) (defined as Eq. (30)) using unstructured hexahedral and tetrahedron elements. As shown, more accurate neutron multiplication factor is obtained from the calculation using unstructured hexahedral elements.

$$RPE(\%)=\frac{calculated\ value-reference\ value}{reference\ value}\times 100. \quad (30)$$

The comparison of calculated power distribution (corresponding to 47612 elements in core modeling) using unstructured hexahedral and tetrahedron [20] elements and reference data [19] in 1/12th of the reactor are given in Tables 4 and 5, respectively. These tables also give the axial distribution of relative power in the different layers. As shown, the results of the developed computer codes and reference values are in a good agreement. However, the calculation using unstructured hexahedral elements give more accurate power distribution in the reactor core.

As shown in Table 3, the calculations are repeated for three different numbers of the elements in order to analyze the sensitivity of the calculations to number the elements. As expected, differences between the calculated neutron multiplication factor and reference value decreases when the number of elements is increased. The calculated RPEs for neutron multiplication factor and power distribution in the present study are in the range of reported results in the similar work [19].

After ensuring the accuracy of static calculations, the three-

Table 3
The calculated neutron multiplication factor for VVER-1000 reactor core.

Number of elements	Tetrahedron	*RPE*(%)	Hexahedral	*RPE*(%)
30148	1.05156	0.19342	1.04983	0.02858
35412	1.05101	0.14102	1.04969	0.01524
47612	1.05078	0.11910	1.04960	0.00667
73892	1.04958	0.00476	1.04953	0.00000

*The reference effective multiplication factor is k_{eff} = 1.04953 [19].

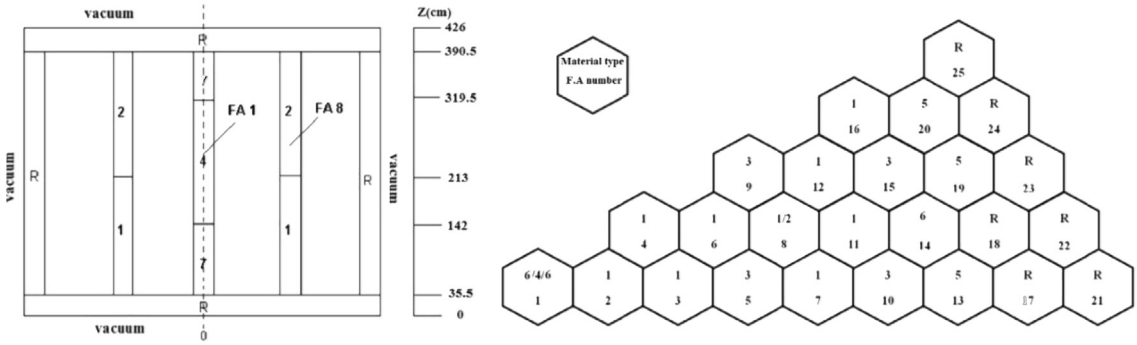

Fig. 2. The 1/12 of the VVER-1000 reactor core.

Table 4
The relative power distribution obtained from unstructured tetrahedron elements for VVER-1000 reactor core by considering the 47612 elements.

FA.	1	2	3	4	5	6	7	8	9	10	Ave	Ref. [19]	RPE(%)
1	0.8679	1.8740	2.3400	1.8660	1.5300	1.1370	0.7703	0.5082	0.3809	0.1648	1.1440	1.1200	2.1420
2	0.6349	1.3790	1.7730	1.7160	1.4410	1.0580	0.7084	0.4562	0.2818	0.1170	0.9565	0.9475	0.9530
3	0.6472	1.4170	1.8720	1.9270	1.6280	1.1450	0.7409	0.4656	0.2694	0.1080	1.0220	1.0140	0.8029
4	0.6307	1.3780	1.8110	1.8490	1.5640	1.1190	0.7323	0.4627	0.2703	0.1091	0.9926	0.9821	1.0640
5	0.8545	1.8740	2.5050	2.6180	2.1810	1.3810	0.8560	0.5323	0.3032	0.1203	1.3220	1.3110	0.8572
6	0.6782	1.4880	1.9840	2.0660	1.7310	1.1470	0.7220	0.4498	0.2570	0.1020	1.0630	1.0570	0.5070
7	0.6664	1.4670	1.9720	2.0780	1.7530	1.1360	0.7194	0.4513	0.2568	0.1013	1.0600	1.0600	−0.0217
8	0.6788	1.4930	2.0040	2.1040	1.7420	0.9338	0.5712	0.3566	0.2028	0.0802	1.0170	1.0090	0.7531
9	0.8469	1.8600	2.4930	2.6160	2.1900	1.3970	0.8711	0.5430	0.3087	0.1222	1.3250	1.3140	0.8565
10	0.7322	1.6100	2.1700	2.3020	2.0100	1.4710	0.9862	0.6268	0.3574	0.1411	1.2410	1.2500	−0.7003
11	0.6303	1.3890	1.8710	1.9810	1.7070	1.1870	0.7792	0.4934	0.2812	0.1108	1.0430	1.0480	−0.5009
12	0.6347	1.3980	1.8820	1.9900	1.7050	1.1700	0.7606	0.4798	0.2733	0.1077	1.0400	1.0410	−0.0797
13	0.3992	0.8769	1.1840	1.2620	1.1180	0.8455	0.5784	0.3701	0.2114	0.0835	0.6928	0.6981	−0.7535
14	0.6010	1.3210	1.7830	1.8970	1.6740	1.2570	0.8563	0.5467	0.3122	0.1233	1.0370	1.0450	−0.7625
15	0.6640	1.4610	1.9710	2.0970	1.8470	1.3780	0.9358	0.5977	0.3414	0.1348	1.1430	1.1510	−0.6995
16	0.5430	1.1970	1.6150	1.7180	1.5120	1.1280	0.7647	0.4883	0.2789	0.1099	0.9355	0.9434	−0.8332
19	0.3489	0.7682	1.0380	1.1070	0.9860	0.7539	0.5206	0.3341	0.1910	0.0755	0.6123	0.6161	−0.6103
20	0.4326	0.9520	1.2860	1.3740	1.2240	0.9364	0.6470	0.4156	0.2377	0.0939	0.7599	0.7631	−0.4233

Table 5
The relative power distribution obtained from unstructured hexahedral elements for VVER-1000 reactor core by considering the 47612 elements.

FA.	1	2	3	4	5	6	7	8	9	10	Ave	Ref. [19]	RPE(%)
1	0.8522	1.8346	2.2898	1.8005	1.4801	1.1036	0.7520	0.4987	0.3817	0.1665	1.1157	1.1200	−0.3671
2	0.6256	1.3536	1.7398	1.6847	1.4181	1.0459	0.7037	0.4555	0.2829	0.1184	0.9427	0.9475	−0.4973
3	0.6392	1.3929	1.8391	1.8968	1.6063	1.1352	0.7391	0.4671	0.2717	0.1097	1.0097	1.0140	−0.4328
4	0.6215	1.3520	1.7754	1.8146	1.5395	1.1051	0.7282	0.4621	0.2718	0.1108	0.9780	0.9821	−0.3971
5	0.8446	1.8442	2.4648	2.5788	2.1558	1.3774	0.8596	0.5384	0.3085	0.1232	1.3095	1.3110	−0.1194
6	0.6717	1.4676	1.9554	2.0382	1.7142	1.1426	0.7235	0.4536	0.2607	0.1049	1.0534	1.0570	−0.3388
7	0.6644	1.4559	1.9562	2.0651	1.7491	1.1436	0.73	0.461	0.2645	0.1056	1.0595	1.0600	−0.0472
8	0.6748	1.4772	1.9818	2.0843	1.7336	0.9171	0.5664	0.3557	0.2038	0.0814	1.0076	1.0090	−0.1366
9	0.8379	1.8334	2.4559	2.5804	2.1674	1.3928	0.8751	0.5487	0.3145	0.1248	1.3130	1.3140	−0.0689
10	0.7351	1.6118	2.1725	2.3103	2.0242	1.4919	1.0068	0.6441	0.3697	0.1472	1.2513	1.2500	0.1027
11	0.6307	1.3858	1.8641	1.9788	1.7104	1.1982	0.7929	0.5055	0.2903	0.1151	1.0471	1.0480	−0.0721
12	0.6341	1.3903	1.8698	1.9795	1.7019	1.176	0.7705	0.4902	0.281	0.112	1.0405	1.0410	−0.0480
13	0.4031	0.8843	1.1938	1.2734	1.1316	0.8602	0.5921	0.3812	0.2191	0.0862	0.7025	0.6981	0.6303
14	0.6057	1.3286	1.7929	1.9105	1.6928	1.2776	0.8763	0.5634	0.3235	0.1285	1.0498	1.0450	0.4574
15	0.6679	1.4645	1.9752	2.1066	1.8620	1.3963	0.9546	0.6144	0.3529	0.1408	1.1535	1.1510	0.2281
16	0.5477	1.2019	1.6196	1.7257	1.5246	1.1435	0.7813	0.5029	0.2904	0.1162	0.9454	0.9434	0.2120
19	0.3509	0.7731	1.0442	1.1162	0.9974	0.7661	0.5315	0.3435	0.1967	0.0774	0.6197	0.6161	0.5843
20	0.4346	0.9544	1.2892	1.3798	1.2324	0.9475	0.6586	0.4250	0.2440	0.0957	0.7661	0.7631	0.3931

dimensional neutron noise calculation was performed. In most papers published in the field of neutron noise analysis, the solution of the neutron noise equation has been performed in the two dimensional geometry [6,8,10,21]. To investigate the variation of the calculated neutron noise distribution by the developed computer code in axial direction, the neutron noise calculation is performed for source type of absorber of variable strength located at X = 31 cm, Y = 19 cm and Z = 177.5 cm. In the present stud, the perturbation (variation of macroscopic cross section) has been considered as $\frac{\delta\Sigma}{\Sigma} = 10^{-5}$. Here, the changes of the neutron noise distribution is investigated in axial direction, while in the previous published work the neutron noise distribution due to neutron noise source of variable strength was only considered in the 2D planes. Fig. 3 shows the calculated neutron noise distribution induced by considered neutron noises source in the layer of reactor core with z = 177.5 cm. The magnitude of neutron noise distribution in the different layers of the reactor core has been presented in Fig. 3. Also, the average values of neutron distribution in the different layers has been given in Fig. 4. As shown, by increasing the distance between the considered layers and the layer that included neutron noise source (z = 177.5 cm), the average of neutron noise distribution decreases. However, the neutron noise distribution (or average value) in the layers close the neutron noise source has remarkable value and it should be considered in the neutron noise analysis. Since the accuracy of calculation of neutron multiplication factor and neutron flux distribution in the reactor core using unstructured hexahedral elements is better than the tetrahedron elements (according to Tables 4 and 5), it is clear that the calculated neutron noise using unstructured hexahedral elements is more accurate than tetrahedron elements ones.

5. Conclusion

The comparison of the calculated neutron multiplication factor and neutron flux distribution using the developed computer codes based on Galerkin Finite Element Method (GFEM) with unstructured hexahedral and tetrahedron elements indicated that the more accurate results could be obtained from the calculation using the unstructured hexahedral elements.

The investigation of the changes of average values of neutron noise distribution in axial direction of the reactor core showed that the 3D neutron noise analysis should be performed instead of 2D. Also, the calculated neutron noise distribution using the unstructured hexahedral elements is more accurate than the tetrahedron

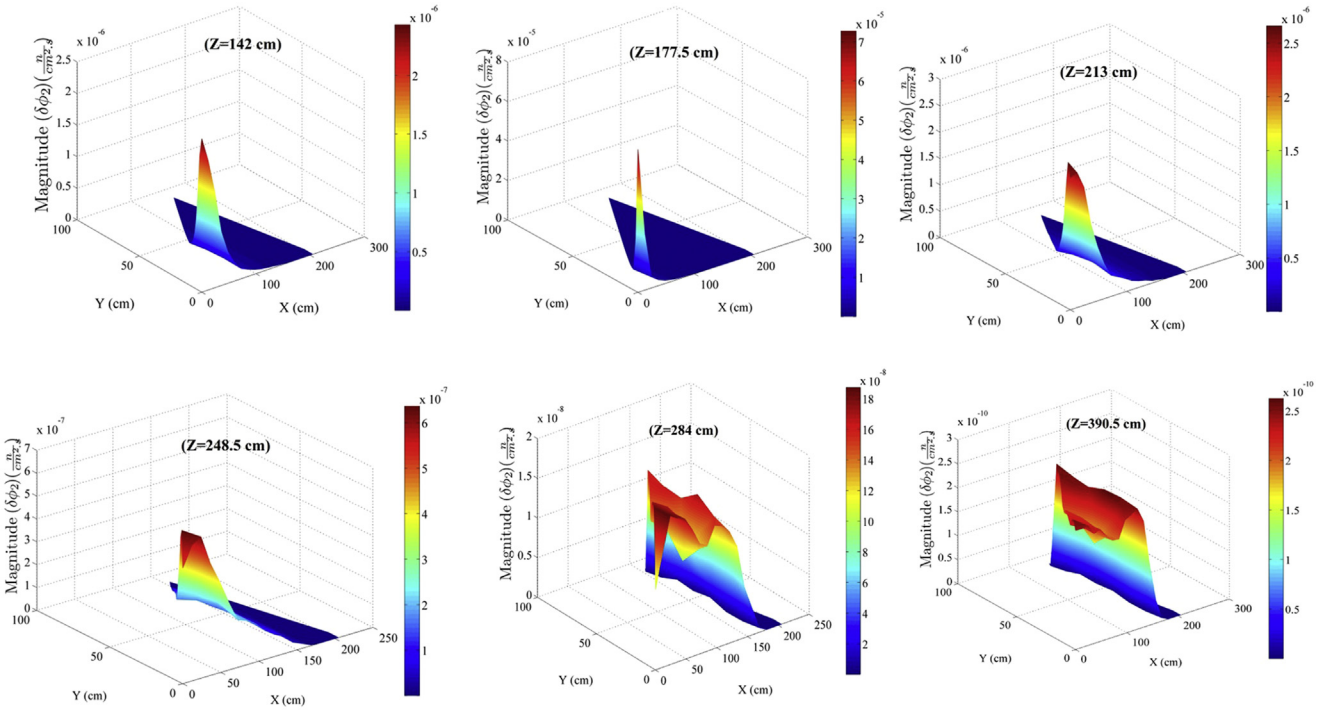

Fig. 3. The neutron noise distribution in the different layers of the reactor core due to the neutron noise source located in layer with Z = 177.5 cm.

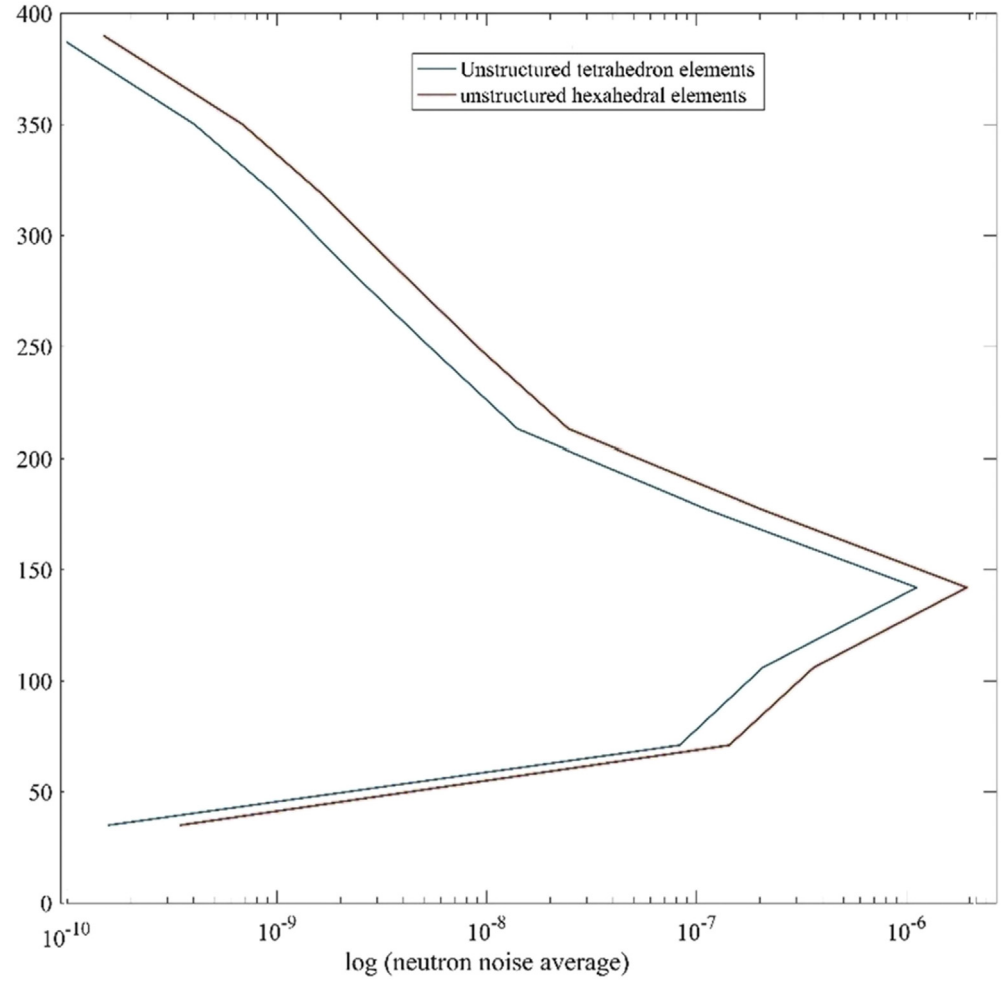

Fig. 4. Variation of average neutron noise in the axial direction.

elements ones.

In summary, we can conclude that both the developed three-dimensional computer codes based on GFEM with unstructured hexahedral and tetrahedron elements give the results with acceptable accuracy in the solution of the neutron diffusion equation and corresponding neutron noise equation. However, the developed computer code using unstructured hexahedral elements is more reliable tool for nuclear reactor core design and its safety analysis.

Acknowledgments

The author is grateful to the research office of the Sharif University of Technology for the support of the present work.

References

[1] M.M.R. Williams, Random Processes in Nuclear Reactors, Elsevier, 2013.
[2] J. Thomas Jr., J. Herr, D. Wood, Noise analysis method for monitoring the moderator temperature coefficient of pressurized water reactors: I. Theory, Nucl. Sci. Eng. 108 (4) (1991) 331–340.
[3] C. Demazière, I. Pázsit, G. Pór, Evaluation of the boron dilution method for moderator temperature coefficient measurements, Nucl. Technol. 140 (2) (2002) 147–163.
[4] C. Demazière, G. Andhill, Identification and localization of absorbers of variable strength in nuclear reactors, Ann. Nucl. Energy 32 (8) (2005) 812–842.
[5] S.A. Hosseini, N. Vosoughi, On a various noise source reconstruction algorithms in VVER-1000 reactor core, Nucl. Eng. Des. 261 (2013) 132–143.
[6] C. Demazière, Development of a 2-D 2-group neutron noise simulator, Ann. Nucl. Energy 31 (6) (2004) 647–680.
[7] V. Larsson, et al., Neutron noise calculations using the Analytical Nodal Method and comparisons with analytical solutions, Ann. Nucl. Energy 38 (4) (2011) 808–816.
[8] H.N. Tran, C. Demazière, Neutron noise calculations in hexagonal geometry and comparison with analytical solutions, Nucl. Sci. Eng. 175 (3) (2013) 340–351.
[9] H.N. Tran, et al., A multi-group neutron noise simulator for fast reactors, Ann. Nucl. Energy 62 (2013) 158–169.
[10] S.A. Hosseini, N. Vosoughi, Neutron noise simulation by GFEM and unstructured triangle elements, Nucl. Eng. Des. 253 (2012) 238–258.
[11] S.A. Hosseini, N. Vosoughi, J. Vosoughi, Neutron noise simulation using ACNEM in the hexagonal geometry, Ann. Nucl. Energy 113 (2018) 246–255.
[12] S.A. Hosseini, F. Saadatian-Derakhshandeh, Galerkin and Generalized Least Squares finite element: a comparative study for multi-group diffusion solvers, Prog. Nucl. Energy 85 (2015) 473–490.
[13] S.A. Hosseini, N. Vosoughi, Development of 3D neutron noise simulator based on GFEM with unstructured tetrahedron elements, Ann. Nucl. Energy 97 (2016) 132–141.
[14] G.I. Bell, S. Glasstone, Nuclear Reactor Theory, US Atomic Energy Commission, Washington, DC (United States), 1970.
[15] S. Itoh, A fundamental study of neutron spectra unfolding based on the maximum likelihood method, Nucl. Instrum. Methods Phys. Res. Sect. A Accel. Spectrom. Detect. Assoc. Equip. 251 (1) (1986) 144–155.
[16] S.A. Hosseini, N. Vosoughi, Noise source reconstruction using ANN and hybrid methods in VVER-1000 reactor core, Prog. Nucl. Energy 71 (2014) 232–247.
[17] I. Pázsit, O. Glöckler, On the neutron noise diagnostics of PWR control rod vibration, I. Periodic vibrations, Nucl. Sci. Eng. 85 (1984) 167–177.
[18] H. Rathod, B. Venkatesudu, K. Nagaraja, Gauss legendre quadrature formulas over a tetrahedron, Numer. Methods Part. Differ. Equ.: Int. J. 22 (1) (2006) 197–219.
[19] G. Schulz, Solutions of a 3D VVER-1000 benchmark, in: Proc. 6-th Symposium of AER on VVER Reactor Physics and Safety, Kirkkonummi, Finland, 1996.
[20] S.A. Hosseini, Development of Galerkin finite element method three-dimensional computational code for the multigroup neutron diffusion equation with unstructured tetrahedron elements, Nucl. Eng. Technol. 48 (1) (2016) 43–54.
[21] S.A. Hosseini, I.E.P. Afrakoti, Neutron noise source reconstruction using the Adaptive Neuro-Fuzzy Inference System (ANFIS) in the VVER-1000 reactor core, Ann. Nucl. Energy 105 (2017) 36–44.